Observations of Deterministic Quantum Correlation Using Coherent Light

Sangbae Kim
Gwangju Institute of Science and Technology
Byoung S. Ham (bham@gist.ac.kr)
Gwangju Institute of Science and Technology

Research Article

Keywords: Quantum correlation, coherent light, Hanbury Brown, Twiss experiments, particle nature of photons, anticorrelation, Bell inequality violation

DOI: https://doi.org/10.21203/rs.3.rs-604290/v1

Observations of deterministic quantum correlation using coherent light

Sangbae Kim and Byoung S. Ham*

School of Electrical Engineering and Computer Science, Gwangju Institute of Science and Technology, Gwangju, South Korea

*bham@gist.ac.kr

(submitted on May 29, 2021)

Abstract:

Complementarity theory is the essence of the Copenhagen interpretation in quantum mechanics. Since the Hanbury Brown and Twiss experiments, the particle nature of photons has been intensively studied for various quantum phenomena such as anticorrelation and Bell inequality violation over the last several decades. Regarding the quantum features based on the particle nature of photons, however, no clear answer exists for how to generate such an entangled photon pair or what causes the maximum correlation between them. Here, we experimentally demonstrate the physics of quantumness on anticorrelation using well defined and nearly sub-Poisson distributed coherent photons, where a particular photon number is post-selected using a photon resolving coincidence measurement technique. As a results, unprecedented wavelength dependent first-order intensity correlation has been observed in the two-photon second-order intensity correlation with 99.9 % visibility, where this result demonstrates the anticorrelation theory in Scientific Reports **10**, 7309 (2020) and opens the door to the on-demand quantum correlation control.

Introduction

Nonclassical quantum features such as Bell inequality violation[1-6] and anticorrelation[7-10] between two-mode quantum particles or engineered individual photon pairs have been intensively studied over the last few decades to understand the quantum nature of entanglement beyond the classical limits of individuality and separability[11]. The physical understanding of quantum entanglement based on the particle nature of photons governed by the energy-time relation via the uncertainty principle has been applied for various quantum information technologies. Although the complementarity theory of quantum mechanics is normally limited to the microscopic world of conjugate entities satisfying the uncertainty principle[11,12], the Schrodinger cat[13-15] as a macroscopic quantum feature should also be confined by the same physics. Here, we report the first observation of on-demand quantum correlation using sub-Poisson distributed coherent photons obtained from an attenuated continuous wave (cw) laser. Since the wave characteristics of such sub-Poisson distributed photons relies on the intrinsic properties of the coherent light source, the degree of quantum correlation among photon pairs can also be deterministically manipulated not only for microscopic entities, but also for a macroscopic Schrodinger cat. This paper opens the door to on-demand quantum entanglement generation from coherent light source if a relative phase is controllable between paired entities.

Since the seminal paper of EPR[16], entanglement representing the maximum correlation between two individual photons or atoms has been demonstrated via the second-order intensity correlation $g^{(2)}(\tau)$, where τ is the time delay between two particles for coincidence detection in an interference scheme[7-11]. Bell inequality violation is for a nonlocal quantum feature in a non-interferometric scheme[1-6], while anticorrelation, the so-called Hong-Ou-Mandel (HOM) dip, is for the same quantum feature in an interferometric scheme[7-10]. If a single photon as a Fock state is considered[17], the phase of a Fock state must be random due to the energy-time relation of the uncertainty principle. Thus, all quantum features denoted by quantum operators in a space-time domain have no definite phase relation between them. This is the fundamental limitation of conventional approach for quantum information. On the contrary, a definite phase relation between paired photons is an essential requirement to understand the fundamental physics of quantum entanglement in a deterministic way. In that sense, the terminology of quantum coherence has been used differently in terms of higher-order correlation[18] ever since the temporal correlation observation between two individual photons was demonstrated by Hanbury Brown and Twiss[19].

Recently, a completely different approach has been pursued for the study of anticorrelation to unveil the quantum nature of photon bunching on a beam splitter (BS)[20,21]. Such a pure coherence optics-based interpretation for a quantum feature has been successful to describe the nonclassical phenomenon of a HOM dip.

As already known, experimental results of Young's double slits or a Mach-Zehnder interferometer (MZI) show the same interference fringe whether the input entities are single photons or coherence lights[22-24]. This is based on Born rule of quantum mechanics regarding superposition of a single photon, where a single photon do not interfere or interact with others, but with itself[25]. The wave-particle duality has been demonstrated for the interference scheme, where the definition of particle-like or wave-like photons is based on coherence[26-28]. As a result, there is no fundamental difference between the wave and particle approaches for a single photon in an interferometric scheme[29]. In the wave approach, self-interference in Young's double-slit experiments or an MZI is the bedrock of all quantum phenomena in an interferometric system regardless of photon numbers or photon characteristics, whether it is interpreted as a particle or a wave. Here, we experimentally demonstrate near-perfect nonclassical second-order intensity correlation using nearly sub-Poisson distributed coherent photons obtained from an attenuated laser to prove recently proposed theory[20]. This is the first step toward on-demand quantum entanglement generation based on the wave nature of photons under the Copenhagen interpretation of quantum mechanics.

Results

An experimental design for on-demand quantum correlation

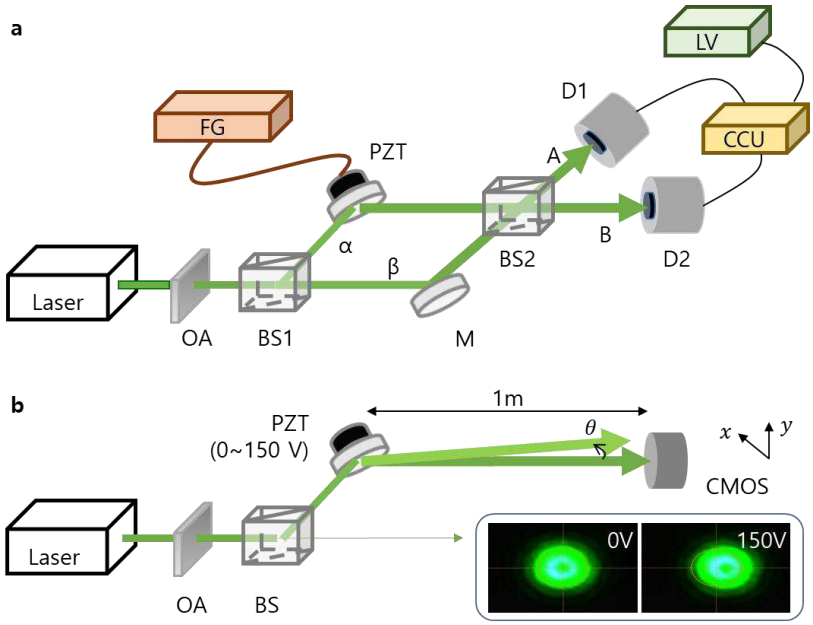

Fig. 1| Schematic of quantum feature generation using post-selected coherent states. a, An interferometric scheme for intensity correlation measurements. **b**, An incoherence driving method using on-demand asymmetric overlap between α and β on BS2 in **a**. OA: optical attenuator, BS: nonpolarizing 50/50/beam splitter, M: mirror. D: single photon counting module; CCU: coincidence counting module; LV: Labview. PZT: Piezo-electric transducer; CMOS: 2D image sensor. Inset: CMOS images, where the solid circle indicates a reference position of the photon (light) α.

Figure 1a shows schematic of the coherent photon-based anticorrelation experiments to prove the theory in ref. 20, where the detected photon numbers are post-selected via coincidence measurements. Unlike conventional spontaneous parametric down conversion (SPDC)-based entangled photons, the coherence length l_c of each photon from a 532 nm laser (Coherent, Verdi-V10) is quite long to be 60 m. The 532 nm laser is continuous wave (cw), whose power stability error is ~1 %. With proper attenuation using neural density filters (OD~10), a nearly sub-Poisson distributed coherent photon stream has been obtained, where the mean photon number is measured at $\langle n \rangle \sim 0.04$ (see Sections A and B of the supplementary Information). The coincidence

measurements in Fig. 1a, however, are not for single photons but for doubly-bunched photons. Because the used single photon counting modules (SPCMs: Excelitas AQRH-SPCM-15) cannot resolve photon numbers, all bunched photons must contribute to the measured data. However, the higher photon number-caused measurement error with three or more bunched photons is negligibly small to be ~1 % according to Poisson statistics as well as measurement results (see Fig. S2 of the Supplementary information). The concept of conventional coincidence detection measurements in Fig. 1a is unrealistic due to the limited scan range (~10 μm) of a Piezo-electric transducer (PZT; Thorlabs, POLARIS-K2S3P) compared with l_c and even unnecessary under the present wave nature approach because the λ-dependet MZI fringe of $g^{(1)}$ correlation is much more sensitive than the τ-dependnet coincidence detection of $g^{(2)}(\tau)$ or a HOM dip[21].

The ultimate purpose of this paper is to investigate the missing $g^{(1)}$ fringe in a HOM dip of $g^{(2)}(\tau)$ measurements to prove the validity of ref. 20. Because Fig. 1a is for a pure coherence optics scheme which is limited to $\tau \ll \tau_c$ in a conventional HOM dip, we need to intentionally induce coherence walk-off via a spatial decoherence technique to set a reference of an incoherence (classical) feature of $g^{(2)}(\tau \gg \tau_c) = 0.5$ (see Section C of the Supplementary Information). Figure 1b is for an intentional incoherence induction scheme via asymmetric control of two-beam overlap on BS2 (see the Inset and Fig. 2). Regarding the asymmetric spatial overlap control, only one axis out of two-axis PZT control unit is scanned by a PZT controller (Thorlabs, MDT693B) to induce intentional decoherence between coincident photon pairs. For this, the PZT at 75 V is set for a good overlap between both beams on BS2 (see Fig. 2). Thus, the present on-demand decoherence control technique gives us a clear understanding of the wave nature of photons via comparison with a conventional τ-based HOM dip scheme[7-10]. Until recently[21], the SPDC-based entangled photon characteristics has been vailed for the anticorrelation as to why the coincidence measurements are λ independent. In fact, the missing $g^{(1)}$ feature in a typical SPDC-based HOM dip is not due to a mysterious quantum phenomenon but because of the entangled photons' characteristics generated from SPDC processes[21].

Very recently, we have experimentally demonstrated that an attenuated coherent single photon has the same bandwidth as the original cw laser light[30]. This is the essence of the self-interference governed by Born rule[29], where the two-photon correlation of a HOM dip is not due to photon interactions but due to superposition of each photon's self-interference on a BS. Regarding the MZI in Fig. 1a, the first BS (BS1) plays a role of a phase shift of $\pi/2$ between the reflected and transmitted photon pairs[31]. This is the first necessary condition for the anticorrelation[20], where the second requirement is randomness or superposition between paired photons[21]. To be clear, the second condition can be satisfied even classically[21] and has not been involved in the present manuscript for simplicity. Under the first condition, thus, the paired photons in Fig. 1a can experience a destructive quantum interference in the second BS (BS2), resulting in photon bunching to either A or B port depending on the PZT-induced phase difference either π or 0, respectively. Unlike general understanding of nondeterministic anticorrelation in most HOM dips, the quantum feature measurements here in this manuscript must be phase dependent, resulting in a deterministic process of quantum correlation. This is the novelty of the present paper to expand and clarify our understanding on quantumness in an interferometric system.

Unlike conventional anticorrelation experiments based on SPDC processes[7], whose generated paired photons have a pre-determined $\pi/2$ phase relation between them[20,21], the attenuated photons in Fig. 1 have the same phase within the narrow bandwidth of 5 MHz. Each MZI output signals $(A; B)$ are detected by a pair of SPCMs $(D_1; D_2)$. The time resolving of the SPCMs is 350 ps at $\lambda = 825$ nm with a dead time of 22 ns, and its dark count rate is measured at 27 ± 5 counts per second (cps). Compared with the present coherence time of a single photon at 0.2 μs, the SPCM's photon resolving time is much shorter, resulting in no bottleneck in $g^{(2)}$ correlation. Both electrically converted single photon signals from the SPCMs are fed into a coincidence counting unit (CCU; Altera DE2) for two-photon coincidence detection measurements.

Figure 2 shows experimental demonstrations for the present decoherence induction method using one-axis controlled PZT in Fig. 1b. For this, the cw power is set at 0.3 μW. The top panels of Fig. 2 represent 2D images captured on a CMOS camera (Thorlabs, DC3241M), while the bottom panels show their corresponding 3D analyses by a manufacturer supplied software. The flat tops of fringes in the bottom panels are due to saturation effect to show the relatively weak side fringes. The second and third columns at 75 V of PZT are for respective

constructive and destructive interferences via delicate tuning of the PZT. At both ends of 0 V and 150 V, multiple fringes result from the intentional asymmetric overlap, corresponding to the incoherence feature for the classical reference. Thus, the spatially misaligned overlap-induced decoherence has successfully demonstrated for a classical reference of an incoherent feature as a function of the PZT scan range.

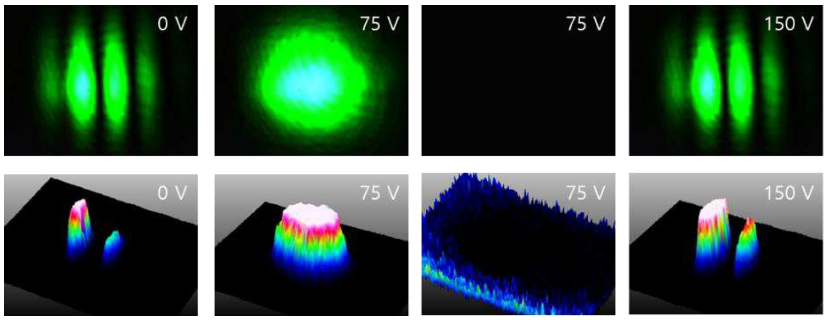

Fig. 2| One-axis PZT controlled coherence modification (see Fig. 1b). (Top) 2D images captured on CMOS (see the inset of Fig. 1**b**). (Bottom) 3D analyses for Top images. The flat top indicates saturated intensity of light.

Preparation of a single photon stream

To provide nearly sub-Poisson distributed single photons, we have analyzed the attenuated photon statistics from the narrow 532 nm laser using two different methods based on SPCMs and a high-speed digital oscilloscope (Yokogawa DL9040; 500 MHz). For these measurements, the photon statistics is pursued in a noninterference regime by simply removing BS2 in Fig. 1. First, we perform photon counting measurements, analyze the obtained data, and compare them with the Poisson statistics for dozens of different OD values from the ND filter combinations. Second, the same measurements are conducted using the oscilloscope to visualize single photon streams, to obtain separate photon statistics, and to compare with the CCU-based ones (see Sections A and B of the Supplementary Information). With these two different measurement techniques, we confirm that the attenuated photon statistics satisfies nearly perfect sub-Poisson distribution for the rests of experiments.

Figure 3 shows captured data from the digital oscilloscope fed by SPCMs. For this, the CCU in Fig. 1 is simply replaced by the digital oscilloscope. The top two rows in Fig 3a show photon streams detected by both SPCMs of D1 (yellow) and D2 (green) in Fig. 1 without BS2, respectively. Figure 3b is an expansion of Fig. 3a for the marked box region. Figure 3c is an expansion of Fig. 3b to show a pair of bunched photons for the marked box. The occurrence rate of bunched photons to single photons in Fig. 3 is $\sim 1\ \%$ for $\langle n \rangle \sim 0.04$. As shown in Section A of the Supplementary Information, the ratio of three or more bunched photons to the doubly-bunched photons is less than 1%. Thus, the doubly-bunched photon pairs are also nearly sub-Poisson distributed within the error of ~1 %.

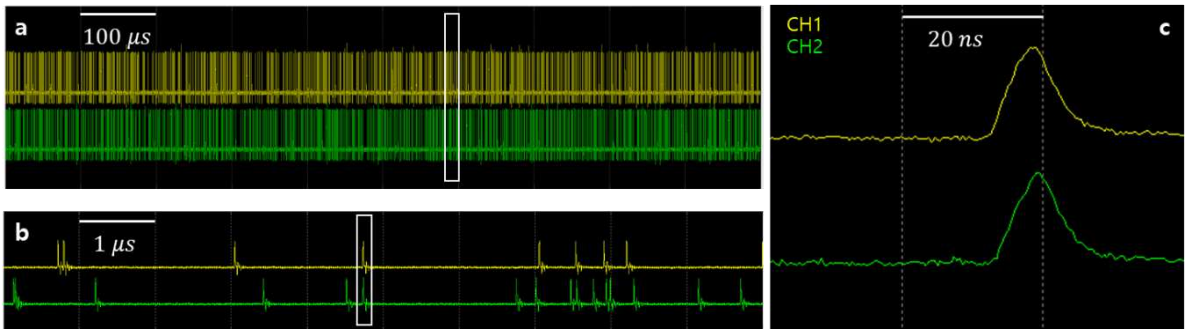

Fig. 3| Sub-Poisson distributed photon characteristics observed by a fast digital oscilloscope. a, Photon streams detected by D1 (yellow) and D2 (green) in Fig. 1 without BS2. **b**, Expansion of the box in **a**. **c**, Expansion of the box in **b** for a coincident (doubly bunched) photon pair.

Observations of nonclassical features using coherent photons

For Fig. 4, the PZT in Fig. 1 is continuously and repeatedly scanned for the same voltage region via a series of saw tooth ramps generated by a function generator (Tecktronics AFG3102; 0~150V), where the center position is fixed for a nearly perfect overlap on BS2, resulting in a symmetric decoherence feature (discussed in Fig. 2) as shown in Fig. 4a. Figure 4a shows only the half of the symmetric PZT scan range originally set for 0~150 V (see Fig. S7 of the Supplementary Information). For the optimum counting rate with respect to the PZT scanning, accumulation time of 0.1 s is set for CCU. Considering ~10 fringes in Fig. 4a, ~200 data points are allocated to each fringe. This corresponds to $\sim 0.01\,\pi$ radians (1.8 degrees) per data point, which is good enough for high resolution measurements of λ dependency in $g^{(2)}$ correlation.

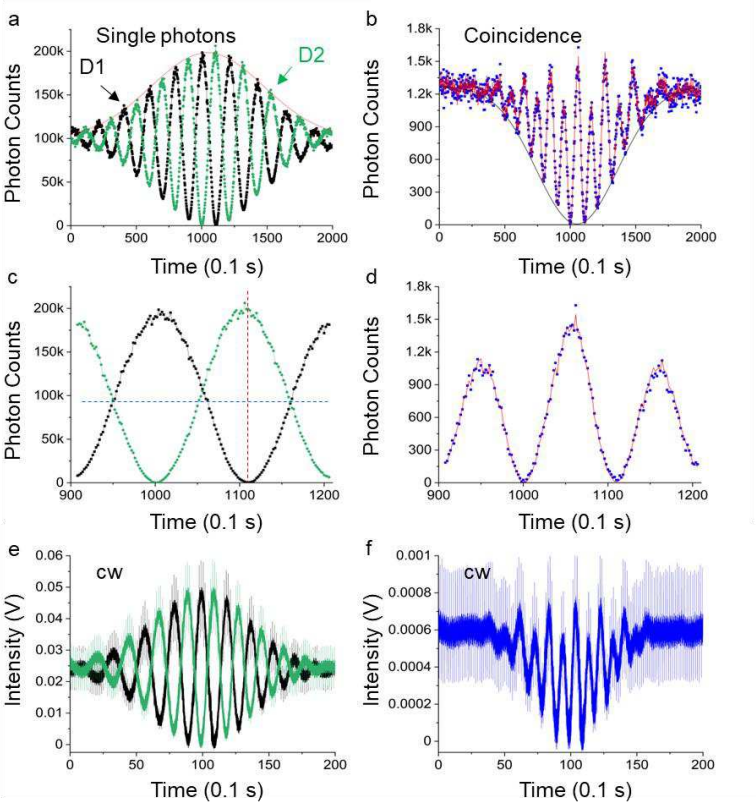

Fig. 4| Experimental results for Fig. 1. a, Single photon counting rates measured by CCU via D1 (black dots) and D2 (green dots) in Fig. 1. **b**, Measured two-photon coincidence counting rates for D1 and D2. **c**,**d**, Respective expansions of **a** and **b**. **e**, Conventional cw MZIs for D1 (black) and D2 (green), where SPCMs are replaced by avalanche photon diodes. **f**, Products of two data points in **e** (performed on the oscilloscope). The cw laser power used for **e** and **f** is 10 μW.

Figure 4a is for individual single photon measurements from both outputs A (D1) and B (D2) in Fig. 1 with BS2. As shown in Fig. 4a, the one-axis PZT scan-induced symmetric decoherence technique is demonstrated successfully, where both ends of the fringes represent incoherence, i.e., the classical bound. Each fringe pattern (black or green dots) from each SPCM shows a typical single photon-based self-interference[30]. The red curve is a Gaussian fit for the measured fringes. Once again, this decoherence feature in Fig. 4a is not from the single photons' characteristics but from the spatial decoherence discussed in Fig. 2. According to the equality between visibility and coherence[32], the asymmetric PZT scan technique in Fig. 1b is confirmed for the intentional decoherence induction as a function of a scan position (time) of PZT for the coincidence measurements. Unlike SPDC generated entangled photons, each MZI output intensity shows a typical MZI fringe governed by $g^{(1)}$ correlation. As mentioned above for the second requirement of anticorrelation, we have not intentionally included randomness of photon superposition, otherwise results in the Gaussian-fit curve without the observed

by $g^{(1)}$ correlation[21]. Reminding of sub-Poisson photon statistics with $\langle n\rangle \sim 0.04$, the deterministic $g^{(1)}$ fringe patterns in Fig. 4a result from self-interference of each photon. The measured single photon's fringe visibility at near center is nearly perfect with 99.9 % from the minimum counts of 105 with respect to the maximum counts of ~200,000.

Figure 4b shows the coincidence detection counts for the doubly bunched photon pairs of Fig. 3c for Fig. 1. The blue dots are the experimental data measured by CCU via two SPCMs. The red fringe curve is for a weighted best-fit curve based on the product of each corresponding data set in Fig. 4a, which is nearly perfectly coincides with the coincidence measurements. This is also a direct proof of $g^{(2)}$ definition of $g^{(1)}$ product average: $g^{(2)}(\tau) = \frac{\langle I_A(t) I_B(\tau+t)\rangle}{\langle I_A(t)\rangle\langle I_B(\tau+t)\rangle}$. Here, this observed fringe pattern of $g^{(2)}$ in Fig. 4b is independent of the randomness via photon superposition required for the second condition of anticorrelation mentioned above. Unlike conventional HOM dip measurements with broadband SPDC generated photons whose SPCM's resolving time is much longer than the photon's coherence time, the present coherent photons have an opposite situation, resulting in no side effect on the detectors. This functional backgrounds with photon characteristics provide near perfect measurement probability except for the quantum efficiency. Thus, the incoherence feature of side bands in Fig. 4 can be treated as an ideal reference of $g^{(2)} = 0.5$ regardless of the actual counting rate. Due to the fact that MZI fringe results from self-interference according to Born rule, there is no discrepancy between single photons and bunched photons in the interferometric fringe in Fig. 4 (see Fig. 4e as an extreme case of cw light). The black Gaussian curve in Fig. 4b is the best-fit curve obtained from the blue dots, where the measured visibility is near perfect and unprecedented, demonstrating the coherent photon-based anticorrelation with a $g^{(1)}$ correlation fringe.

The minimum photon counting rate in Fig. 4b at center is 2 counts per 0.1 s, which is within the dark count rate of 5 per 0.1 s of the SPCM. Due to the intentional setup of decoherence with the asymmetric PZT scanning method, all maxima in Fig. 4b indicate the classical lower bound of $g^{(2)} = 0.5$. According to the weighted product of individual data in Fig. 4b (see the red curve), all crossing points between the black and green dots in Fig. 4a should coincide with the maxima in Fig. 4b, indicating a phase dependent incoherence feature of the coherent photons (discussed in Fig. 5). Thus, all measurement data points below the maxima at ~1,300 counts per 0.1 s represent a quantum feature. Thus, Fig. 4b clearly demonstrates new physics of the wave nature-based anticorrelation whose characteristics is phase dependent. This new physics of anticorrelation with sub-Poisson distributed coherent photons expands our understanding on quantum mechanics and opens the door to on-demand quantum information processing.

On the contrary of conventional HOM dips based on SPDC-generated entangled photon pairs, the coincidence measurements in Fig. 4b results in λ dependency as proposed in ref. 20. The λ dependency implies deterministic manipulation of quantum correlation. This striking observation confirms the existence of a specific phase relation φ between the paired entangled photons in SPDC, where the anticorrelation occurs at $\varphi = \pm\pi/2$ as theorized in ref. 20. The mismatching between Fig. 4b and conventional HOM dips has been fully analyzed recently under the same physics via coherence washout among symmetrically detuned paired photons generated from SPDC[21].The matched intensity product-based best fit curve with the coincidence measurements fully supports the present photon number-independent wave approach for quantum mechanics.

Figures 4c and 4d are expansions of Figs. 4a and 4b, respectively. As shown in Fig. 4c, both fringes of single photon measurements are not perfectly aligned (see the horizontal dotted line). Such misalignment is due to the imperfect overlap on BS2, intensity fluctuation of the laser, or MZI phase fluctuation by air turbulence. As a result, the maxima of intensity correlation in Fig. 4d, i.e., the crossing point products in Figs. 4c fluctuate, too. As analyzed in Fig. S8 of the Supplementary Information, this fluctuation, however, is within 1 % misalignment error (discussed in Fig. 5).

Figures 4e and 4f are for the corresponding cw cases of Figs. 4a and 4b, respectively. For this, the SPCMs in Fig. 1 is replaced by avalanche photon diodes (Thorlabs, APD 110A) and connected directly to the oscilloscope (YOKOGAWA DL9040) used in Fig. 3. The plots of Figs. 4e and 4f are from the stored data in the oscilloscope. Both black and green fringes in Fig. 4e are from both APDs corresponding to the outputs A and B in Fig. 1, respectively. Figure 4f is generated using the product function of the oscilloscope for the data in Fig. 4e, which corresponds to the red curve in Fig. 4b. Because the physics of the present anticorrelation is based on the wave nature of photons, there should be no difference between coincidence measurements of single photons

in Fig. 4b and conventional wave optics of MZI outputs in Fig. 4f. According to Born rule of quantum mechanics regarding self-interference, the MZI in Fig. 1 limits the path superposition to the case of a single photon-two slit system, where the coincidence measurement should be the same as the weighted product of each single photon measurement[22-24]. This rule is also applied to the conventional SPDC-based anticorrelation, where the HOM dip is caused by photon bunching due to destructive interference in an MZI between two self-interferences in Figs. 4b and 4f[20,21]. As already demonstrated by Born rule tests[29], Fig. 4 also demonstrates Born rule of quantum mechanics that there is no difference between the particle (single) and wave (cw) natures of photons in an interferometric scheme. This experimental demonstration for two-photon coincidence measurements in Fig. 4b is unprecedented and opens the door to new physics of deterministic quantum correlation.

Figure 5 provides reconfigured data from Fig. 4a for the perfect overlap of the observed nonclassical features. For this, all data from D1 in Fig. 4a are moved by two pixel points out of 2000 points in a row, resulting in nearly equal maxima as shown in Fig. 5b, resulting from the nearly perfect crossing points in Fig. 5a. As discussed by the logic gate operation and coherence optics in Fig. 4b, Fig. 5b shows a perfect coincidence detection rates for anticorrealtion with ~100% visibility, whose nonclassicality is φ dependent. Figures 5c and 5d are numerical simulations corresponding to Figs. 5a and 5b, respectively, with sine and cosine functions multiplied by a Gaussian function, representing the MZI outputs (see Fig. S8 of the Supplementary Information). The coincidence rate in Fig. 5d is normalized for the product of D1 and D1 in Fig. 5a. Here, the meaning of the same maxima is self-evident by the definition of product between D1 and D2 for AND gate operation in CCU as well as $g^{(2)}$ correlation. The maxima (minima) in Fig. 5b reveals the perfect incoherent (coherent) characteristics as a classical (quantum) bound. Except for maxima in Figs. 5b, all data points are nonclassical by definition of $g^{(2)}$ correlation in quantum mechanics due to the preset reference of maxima. Thus, the observed quantum correlation in Fig. 4b is strongly related with a relative phase between paired photons, resulting in on-demand control of quantum features. The maximum anticorrelation with zero coincidence count rate occurs at the MZI phase basis, $\varphi \in \{0, \pi\}$. This phase basis relation is the essence for the fundamental physics of quantum correlation.

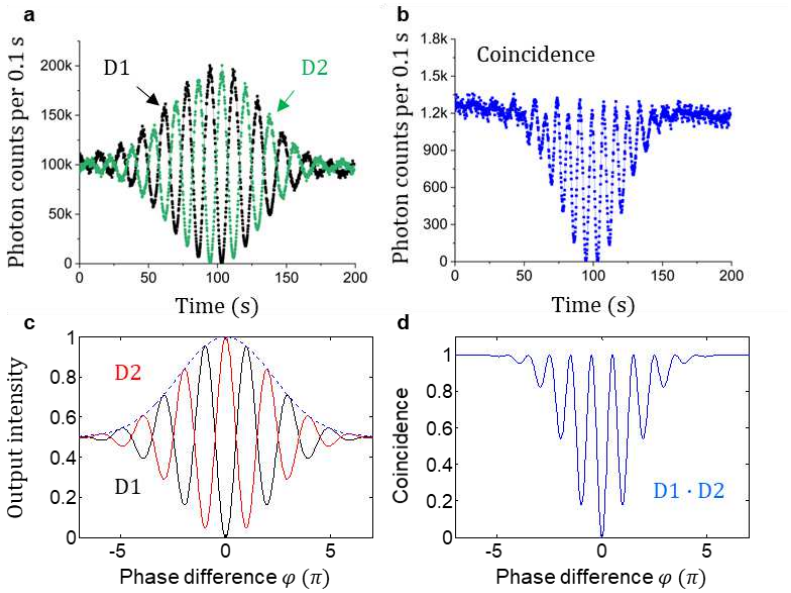

Fig. 5| Analysis of quantum correlation based on coherent photons. a,**b**, All D1 data in Fig. 4**a** are shifted by two pixel points out of 2000 points. **c**,**d**, Numerical simulations for **a** and **b**, respectively. The coincidence value in **d** is normalized.

Conclusion

We experimentally demonstrated λ-dependent two-photon correlation using nearly sub-Poisson distributed coherent photons and compared the results with conventional SPDC-based HOM dips. The λ dependency in coincidence measurements reveals new physics of quantum features interpreted by the wave nature of photons without violating quantum mechanics. Unlike conventional nondeterministic quantum features based on the particle nature of photons, the observed $g^{(1)}$ fringe in the two-photon coincidence measurements directly proves the phase basis-caused interpretation of quantum mechanics, resulting in deterministic manipulations of quantum correlations. For the demonstrations of anticorrelation using coherent photons, a simple MZI scheme was used, where the first BS plays a role of a $\pi/2$ phase shift between coincident photon pairs demonstrating the phase relation between entangled photon pairs interacting on a BS. To induce an artificial incoherence effect for a classical bound, an asymmetric PZT scanning method was developed, otherwise a long coherence time makes meaningless coincidence detection because all photons are coincident at any time of the MZI scanning regime. For coincidence detection measurements between two output ports of the MZI, we confirmed the new physics of anticorrelation proposed in ref. 20 by demonstrating near perfect visibilities (99.9%) in the coincidence measurements, where phase dependent interference fringe appeared. To support the experimental data, a simple Gaussian adjusted MZI simulations were compared, resulting in a near perfect coincidence with the experimental data. Thus, the observed coincidence measurements based on phase controlled coherent photons opens the door to the deterministic control of quantum features without violating quantum mechanics. Moreover, the present demonstration witnesses the new interpretation of quantum mechanics, satisfying Copenhagen interpretation of the wave-particle duality as well as self-interference of Born rule. By replacing the single photons with a cw laser, the thumb rule of no distinction between quantum particles and classical waves in an interferometric scheme by the Born rule tests was experimentally demonstrated via the concept of self-interference. This result opens the door to deterministic quantum information science compatible with coherence optics.

Reference

1. Bell, J. On the Einstein Podolsky Rosen Paradox. *Physics* **1**, 195-290 (1964).
2. Clauser, J. F., Horne, M. A., Shimony, A. & Holt, R. A. Proposed experiment to test local hidden-variable theories. *Phys. Rev. Lett.* **23**, 880–884 (1969).
3. Brunner, N. et al. Bell nonlocality. *Rev. Mod. Phys.* **86**, 419–478 (2014).
4. Kwiat, P. G., Steinberg, A. M. & Chiao, R. Y. High-visibility interference in a Bell-inequality experiment for energy and time. *Phys. Rev. A* **47**, R2472–R2475 (1993).
5. Solano, E., Matos Filho, R. L. & Zagury, N. Deterministic Bell states and measurement of motional state of two trapped ions. *Phys. Rev. A* **59**, R2539–R2543 (1999).
6. Hensen, B. et al. Loophole-free Bell inequality violation using electron spins separated by 1.3 kilometers. *Nature* **526**, 682-686 (2015).
7. Hong, C. K., Ou, Z. Y. & Mandel, L. Measurement of subpicosecond time intervals between two photons by interface. *Phys. Rev. Lett.* **59**, 2044-2046 (1987).
8. Ou, Z. Y., Gate, E. C., Magill, B. E. & Mandel, L. Fourth-order interference technique for determining the coherence time of a light beam. *J. Opt. Soc. Am.* B **6**,100-103 (1989).
9. Kim, H., Kwon, O. & Moon, H. S. Experimental interference of uncorrelated photons. *Sci. Rep.* **9**, 18375 (2019).
10. Deng, Y.-H. et al. Quantum interference between light sources separated by 150 million kilometers. *Phys. Rev. Lett.* **123**, 080401 (2019).
11. Bertet, P. et al. A complementarity experiment with an interferometer at the quantum-classical boundary. *Nature* **411**, 166–170 (2001).
12. Bohr, N. in *Albert Einstein: Philosopher Scientist* (ed. Schilpp, P. A.) 200-241 (Library of Living Philosophers, Evanston, 1949); reprinted in *Quantum Theory and Measurement* (eds Wheeler, J. A. & Zurek, W. H.) 9-49 (Princeton Univ. Press, Princeton, 1983).
13. Giovannetti, V., Lloyd, S. & Maccone, L. Quantum-enhanced measurements: beating the standard quantum limit. *Science* **306**, 1330–1336 (2004).
14. Wang, X.-L. et al. 18-qubit entanglement with six photons' three degree of freedom. *Phys. Rev. Lett.* **120**, 260502 (2018).

15. Pezze, L. et al. Quantum metrology with nonclassical states of atomic ensemble. *Rev. Mod. Phys.* **90**, 035005 (2018).
16. Einstein, A., Podolsky, B. & Rosen, N. Can quantum-mechanical description of physical reality be considered complete? *Phys*. *Rev.* **47**, 777–780 (1935). (1935).
17. Chu, Y., Kharel, P., Yoon, T., Frunzio, L., Rakich, P. T. & Schoelkopf, R. J. Creation and control of multi-phonon Fock states in a bulk acoustic-wave resonator. *Nature* **563**, 666-670 (2018).
18. Glauber, R. J. The quantum theory of optical coherence. *Phys. Rev.* **130**, 2529-2539 (1963).
19. Hanbury Brown R. and Twiss, R. Q. A test of new type of stellar interferometer on Sirius. *Nature* **178**, 1046-1048 (1956).
20. Ham, B. S. The origin of anticorrelation for photon bunching on a beam splitter. *Sci. Rep.* **10**, 7309 (2020).
21. Ham, B. S. Coherently controlled quantum features in a coupled interferometric scheme. *Sci. Rep*. **11**,11188 (2021).
22. Grangier, P., Roger, G. & Aspect, A. Experimental evidence for a photon anticorrelation effect on a beam splitter: A new light on single-photon interference. *Europhys. Lett.* **1**, 173–179 (1986).
23. Pleinert, M.-O., Rueda, A., Lutz, E. & voa Zanthier, J. Testing higher-order quantum interference with many-particle states. *Phys. Rev. Lett*. **126**, 190401 (2021).
24. Sorkin, R. D. Quantum mechanics as quantum measure theory. *Mod. Phys. Lett*. A **9**, 3119-3127 (1994).
25. Dirac P A M *The principles of Quantum mechanics* (4th ed., Oxford university press, London, 1958), Ch. 1, p. 9.
26. Kim, Y.-H., Yu, R., Kulik, P., Shih, Y. & Scully, M. O. Delayed "choice" quantum eraser. *Phys. Rev. Lett.* **84**, 1-5 (2000).
27. Peruzzo, A., Shadbolt, P., Brunner, N., Popescu, S. & O'Brien, J. L. A quantum delayed-choice experiment. *Science* **338**, 634–637 (2012).
28. Kaiser, F., Coudreau, T., Milman, P., Ostrowsky, D. B. & Tanzilli, S. Entanglement-enabled delayed-choice experiments. *Science* **338**, 637-640 (2012).
29. Sinha, U., Couteau, C., Jennewein, T., Laflamme, R. & Weihs, G. Rulling out multi-order interference in quantum mechanics. *Science* **329**, 418-420 (2010).
30. Kim, S. & Ham, B. S. "Revisiting self-interference in Young's double-slit experiments," arXiv:2104.08007 (2021).
31. Degiorgio,V. Phase shift between the transmitted and the reflected optical fields of a semireflecting lossless mirror is π/2. *Am. J. Phys.* **48**, 81–82 (1980).
32. L. Mandel and E. Wolf, *Optical coherence and quantum optics*. Ch. 8. Cambridge University Press (New York, 1995).

Methods

A standard Mach Zehnder interference (MZI) test is performed using an unattenuated cw laser of Coherent Verdi V10 at $\lambda = 532$ nm, whose spectral bandwidth is 5 MHz. For the sub-Poissonian distributed single photon generations, conventional coincidence measurement technique is applied. To confirm the sub-Poissonian distributed photon statistics, photon visualization is additionally conducted using a fast digital oscilloscope (YOKOGAWA DL9040; 500 MHz; 400 ps resolving time for two-channel access). For this, the SPCMs are directly connected to the oscilloscope. The size of the MZI in Fig. 1 is $\sim 10\text{x}10 cm^2$, enclosed by a cartoon box to minimize air fluctuation-caused phase noise. Because the bandwidth-caused coherence length of the laser is long enough to be 60 m, the PZT-caused MZI interference fringes observed in Figs. 2-5 are well defined within the PZT length variations of a few microns. For conventional cw MZI tests in Fig. 4e and 4f, the SPCM for D2 is replaced by an avalanche photon diode (Thorlabs, APD 110A) and directly connected to the oscilloscope.

1. Dark count measurements for a single photon detection module

In a dark room condition enclosed by a black cartoon box, both single photon counting modules (Excelitas AQRH-SPCM-15) are tested for the dark count rate of 27 ± 5 (counts/s) without input photons, which is satisfied with the manufacture specification of 50 (count/s).

2. Attenuated 532 nm laser

The attenuated light source is Coherent cw laser (Verdi V10). The output intensity is stabilized at ~1 % variation for the fixed output power of 10 mW. For the cw MZI experiments in Fig. 4, OD 3 of ND filters are placed before MZI, resulting in $10\ \mu W$. For the single photon MZI experiments in Figs. 2~5, another OD 10 is added, resulting in $1\ fW$ power and a mean photon number of $\langle n \rangle \sim 0.04$.

3. Counting method for single and bunched photons by a coincidence counting module

The SPCM-generated electrical pulses are sent to the coincidence counting module (CCU: DE2 FPGA, Altera). The pulse duration of each electrical signal from SPCM for single photon detection is ~10 ns. Both single and coincidence counting numbers are counted in parallel by DE2 for 100 ms acquisition time for each data point, otherwise specified. The measured data is transferred to Labview via RS232 cable for a coincidence_rs232(4_5).vi application program in real time. For single and coincidence measurements in Fig. 4, the measured photon number is compared with that by an oscilloscope-based visualization technique below. The acquisition time of 100 ms for the CCU was set for an optimum number between the MZI fringe duration and the counted coincidence detections. Additionally, photon statistics for single photons, doubly bunched, and triply bunched photons, a conventional photon resolving measurement technique are used. The results are shown in Fig. S2 of the Supplementary Information. In this data, higher-order bunched photon ratio to the doubly bunched photons is less than 1 %. The mean photon number is measured at $\langle n \rangle = 0.04$.

4. Counting method for single and bunched photons by a fast digital oscilloscope

For this, SPCMs were directly connected to the oscilloscope (YOKOGAWA; DL9040). Channel 1 of the oscilloscope is for D1, while Channel 2 is for D2. Due to the storage limitations of the oscilloscope for a displaced wave form on a screen, a stored 1 ms data length is analyzed for both sub-Poissonian photon distribution and coincidence detections. The results are also compared with the SPCM-based photon statistics. To count single photons in each data set, a homemade MATLAB program is used (see code in Fig. S6 of the Supplementary Information). For 10 measured data samples (not shown), the counted numbers for single photons are tabulated in Table S3 of the Supplementary Information.

5. Asymmetric PZT scanning

The coherence-length modification technique in Fig. 1b is based on the linearly increased phase shift via walk-off cross section between two lights on BS2 in Fig. 1, where such misalignment is conducted by an asymmetric control of a PZT kinematic mirror (Thorlabs, POLARIS-K2S3P) via a PZT controller (Thorlabs, MDT693B). For this, a PZT scanning applies to one of two mirror control knobs, where the midpoint of the scanning range is set to be maximally coherent at 75 V, whose PZT voltage resolution is 1.5 mV.

Data availability

Data for figures are available upon reasonable requests.

Acknowledgments This work was supported by GIST via GRI 2020.

Author contributions B.S.H. conceived the research on both theory and experiments, did numerical simulations, data analysis, and wrote the manuscript; S.K performed all experiments and analyzed the related data.

Correspondence and request of materials should be addressed to BSH (email: bham@gist.ac.kr).

Competing interests The author declares no competing (both financial and non-financial) interests.

Supplementary information is available in the online version of the paper.

Figures

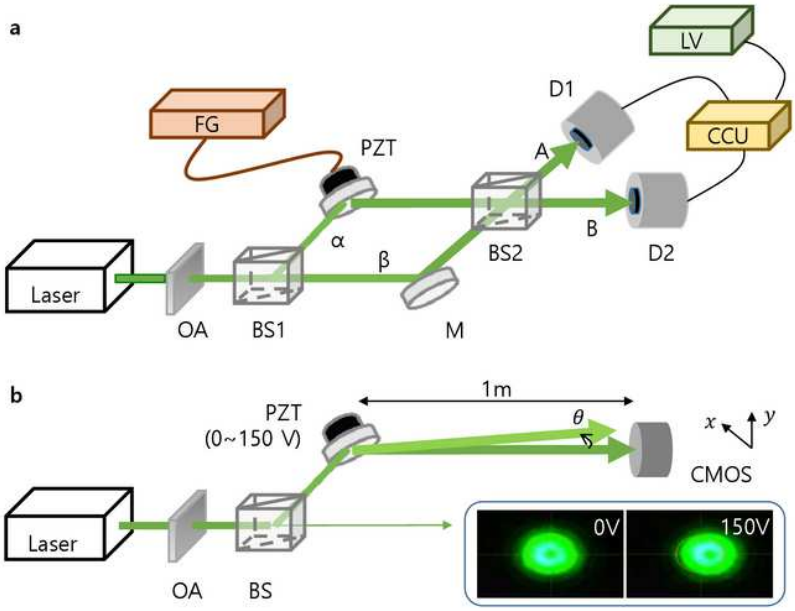

Figure 1

Schematic of quantum feature generation using post-selected coherent states. a, An interferometric scheme for intensity correlation measurements. b, An incoherence driving method using on-demand asymmetric overlap between α and β on BS2 in a. OA: optical attenuator, BS: nonpolarizing 50/50/beam splitter, M: mirror. D: single photon counting module; CCU: coincidence counting module; LV: Labview. PZT: Piezo-electric transducer; CMOS: 2D image sensor. Inset: CMOS images, where the solid circle indicates a reference position of the photon (light) α.

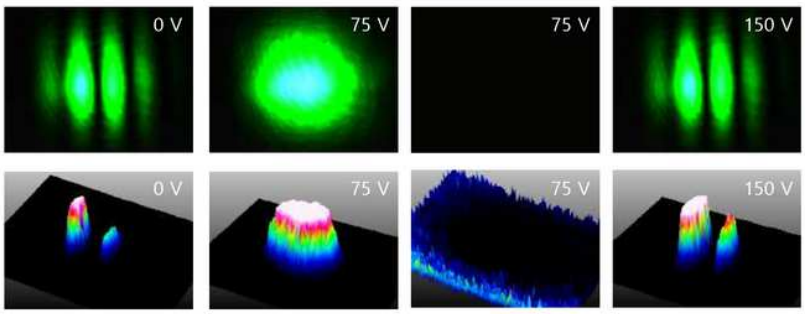

Figure 2

One-axis PZT controlled coherence modification (see Fig. 1b). (Top) 2D images captured on CMOS (see the inset of Fig. 1b). (Bottom) 3D analyses for Top images. The flat top indicates saturated intensity of light.

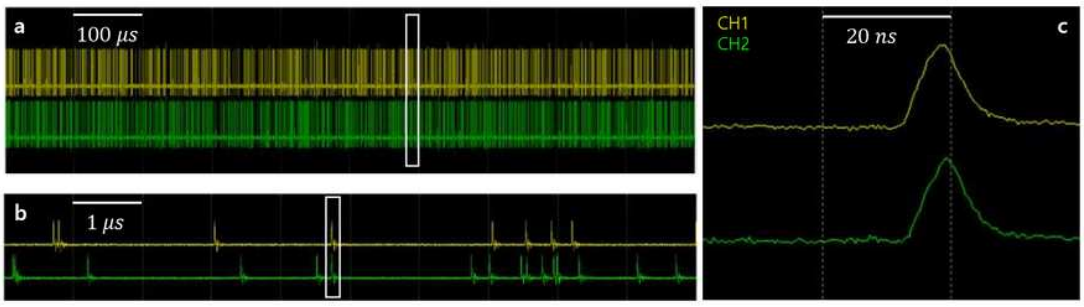

Figure 3

Sub-Poisson distributed photon characteristics observed by a fast digital oscilloscope. a, Photon streams detected by D1 (yellow) and D2 (green) in Fig. 1 without BS2. b, Expansion of the box in a. c, Expansion of the box in b for a coincident (doubly bunched) photon pair.

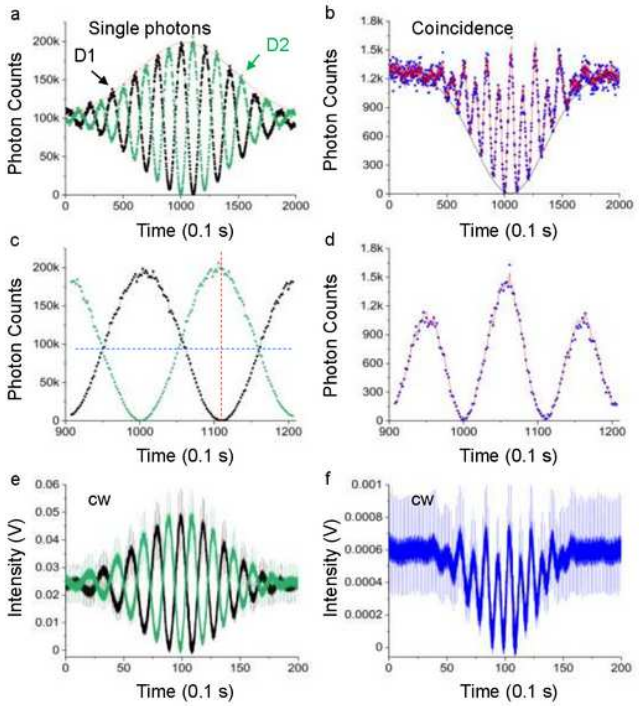

Figure 4

Experimental results for Fig. 1. a, Single photon counting rates measured by CCU via D1 (black dots) and D2 (green dots) in Fig. 1. b, Measured two-photon coincidence counting rates for D1 and D2. c,d, Respective expansions of a and b. e, Conventional cw MZIs for D1 (black) and D2 (green), where SPCMs are replaced by avalanche photon diodes. f, Products of two data points in e (performed on the oscilloscope). The cw laser power used for e and f is 10 μW.

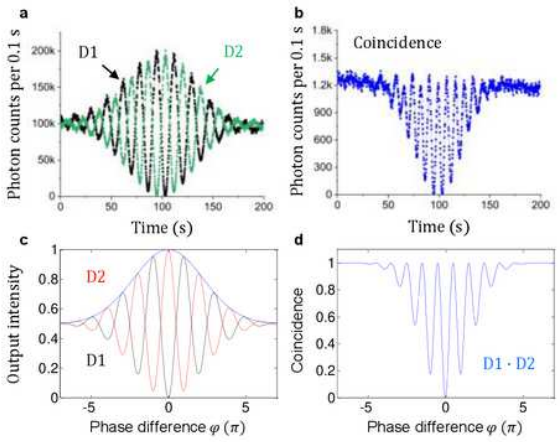

Figure 5

Analysis of quantum correlation based on coherent photons. a,b, All D1 data in Fig. 4a are shifted by two pixel points out of 2000 points. c,d, Numerical simulations for a and b, respectively. The coincidence value in d is normalized.

Supplementary Files

This is a list of supplementary files associated with this preprint. Click to download.

- SupplementaryInformation0529r.pdf